Optimization of Subgridding Schemes for FDTD

Shumin Wang, Fernando L. Teixeira, Robert Lee, and Jin-Fa Lee

***Abstract*—A procedure to optimize the coupling coefficients between fine and coarse mesh regions for two-dimensional (2-D) finite-difference time-domain (FDTD) subgridding algorithms is introduced. The coefficients are optimized with respect to different angles and expanded in a form suitable for FDTD computation.**

***Index Terms*—FDTD method, subgridding.**

I. Introduction

TO BETTER model problems with disparate geometrical sizes, mesh refinement is often used in partial differential equation (PDE) based methods. Mesh refinement allows for the use of different cells sizes over different regions in the mesh and are instrumental in saving computational resources. In the finite-difference time-domain (FDTD) method, these algorithms are usually referred to as *subgridding* algorithms, e.g., [1]–[5]. However, because of the hyperbolic nature of time-domain equations, the fine and coarse mesh regions need to be adequately coupled at their respective boundaries. Usually, spurious reflections are produced at those boundaries due to the mismatch in both the discrete wave numbers and discrete impedances at each region (both of which depend on the cell size). In this work, we introduce a systematic way to optimize the coupling coefficients for two-dimensional (2-D) subgridding algorithms in order to minimize the spurious reflections over a broad range of frequencies.

II. Subgridding Algorithm

Fig. 1 depicts the TE_z case of the 2-D-subgridding algorithm with a coarse-to-fine refinement ratio of $3:1$. Capital letters denote coarse region fields and lower case letters denote fine region fields. Although not strictly necessary, odd ratios are convenient to yield collocated H_z fields and preserve dual grid symmetry. Moreover, to avoid large impedance mismatching, we focus on the $3:1$ case. If a higher refinement ratio is needed, the algorithm could be applied successively. For stability concerns, we use the same time step in coarse and fine domains and explicitly enforce reciprocity in the field update [6], [7] at the coarse/fine transition region.

The subgridding algorithm consists of five steps. 1) At time t_i, $E_y(t_i)$ is calculated in the coarse region up to the location indexed by 0 in Fig. 1. 2) Using spatial interpolation, the missing h_z are obtained at time $t_i - \delta t/2$ at the location indexed by 1.5. For collocated field components, the coarse region values are used directly. 3) The ordinary Yee's algorithm is applied to update the e and h fields in the fine region from the locations indexed by 2 and above at time t_i and $t_i + \delta t/2$, respectively. 4) Reciprocity is used to calculate $H_z(t_i + \delta t/2)$ at the location indexed by 1.5. Other $H_z(t_i + \delta t/2)$ in the coarse region are also calculated by ordinary Yee's algorithm. 5) Let $i = i + 1$.

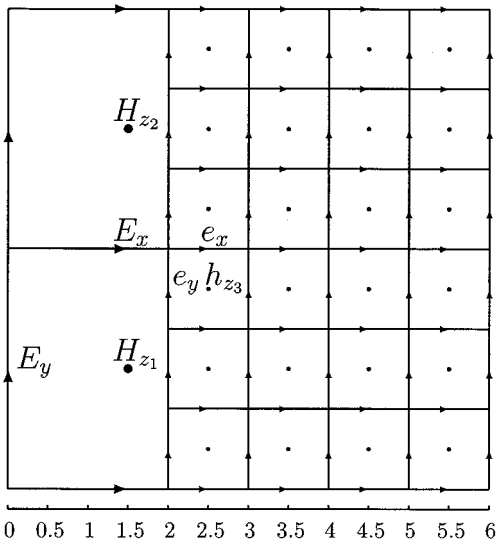

Fig. 1. Coarse–fine region boundary.

III. Optimization

A. Three-Point Coupling Scheme

In the above subgridding scheme, mesh coupling occurs when obtaining h_z at the location indexed by 1.5 in Fig. 1. We assume a nearest neighbor three-point coupling for e_y at location indexed by 2 in the general form

$$e_y = C_1 H_{z1} + C_2 H_{z2} + C_3 h_{z3}. \tag{1}$$

Inserting the plane wave solutions (eigenfunctions in the continuum limit) of Maxwell's equations, we obtain

$$H_{z1} = \eta^{-1} E_0 e^{jkh\cos(\theta)/6} e^{jkh\sin(\theta)/3} \tag{2}$$

$$H_{z2} = \eta^{-1} E_0 e^{jkh\cos(\theta)/6} e^{-2jkh\sin(\theta)/3} \tag{3}$$

$$h_{z3} = \eta^{-1} E_0 e^{-jkh\cos(\theta)/6} \tag{4}$$

$$e_y = E_0 \cos\theta \tag{5}$$

where h is the cell size in coarse region, k is the wave number, E_0 is the magnitude of the electric field, η is the wave impedance, and θ is the incident angle with respect to the

Manuscript received November 13, 2001; revised March 21, 2002. This work was supported in part by the NRC under Contract NRC-CR-96-0013 and OSU-RF under Grant SG-101139. The review of this letter was arranged by Associate Editor Dr. Shigeo Kawasaki.

The authors are with the ElectroScience Laboratory and Department of Electrical Engineering, The Ohio State University, Columbus, OH 43212 USA (e-mail: wangs@ee.eng.ohio-state.edu).

Publisher Item Identifier S 1531-1309(02)05769-0.

positive x-axis. The relative location of H_{z1}, H_{z2}, and h_{z3} is depicted in Fig. 1. Substituting (2)–(5) into (1), we obtain

$$\eta\cos\theta = C_1 e^{jkh\cos(\theta)/6} e^{jkh\sin(\theta)/3} + C_2 e^{jkh\cos(\theta)/6} \cdot e^{-2jkh\sin(\theta)/3} + C_3 e^{-jkh\cos(\theta)/6}. \quad (6)$$

To solve for the coefficients in (6), we employ the ansatz below

$$\int_0^{2\pi} \delta(\theta)\,d\theta = 0$$
$$\int_0^{2\pi} \delta(\theta)\sin(\theta)\,d\theta = 0$$
$$\int_0^{2\pi} \delta(\theta)\cos(\theta)\,d\theta = 0 \quad (7)$$

where

$$\delta(\theta) = \eta\cos\theta - \left[e^{jkh\cos(\theta)/6}\left(C_1 e^{jkh\sin(\theta)/3} + C_2 e^{-2jkh\sin(\theta)/3}\right) + C_3 e^{-jkh\cos(\theta)/6}\right] \quad (8)$$

defines the coupling error. Since $\delta(\theta)$ can be expanded in a Fourier series in terms of $\cos(n\theta)$ and $\sin(n\theta)$, it is clear that (7) is equivalent to enforcing the first three terms in the series to be zero. The remaining terms in the series are proportional to integrals on the form $\int_0^{2\pi} e^{j[\alpha\cos(\theta)+\beta\sin(\theta)]}\sin(n\theta)\,d\theta$ and $\int_0^{2\pi} e^{j[\alpha\cos(\theta)+\beta\sin(\theta)]}\cos(n\theta)\,d\theta$ and can be expressed in terms of first kind Bessel functions $J_n(x)$ with real argument $|x| < 1/2$. This is because

$$\int_0^{2\pi} e^{j[\alpha\cos(\theta)+\beta\sin(\theta)]}\sin(n\theta)\,d\theta = \begin{cases} j2\pi\cos(n\theta_0)J_n\left(\sqrt{\alpha^2+\beta^2}\right), & \text{for odd } n \\ -2\pi\sin(n\theta_0)J_n\left(\sqrt{\alpha^2+\beta^2}\right), & \text{for even } n \end{cases}$$

$$\int_0^{2\pi} e^{j[\alpha\cos(\theta)+\beta\sin(\theta)]}\cos(n\theta)\,d\theta = \begin{cases} j2\pi\sin(n\theta_0)J_n\left(\sqrt{\alpha^2+\beta^2}\right), & \text{for odd } n \\ 2\pi\cos(n\theta_0)J_n\left(\sqrt{\alpha^2+\beta^2}\right), & \text{for even } n \end{cases}$$

where $\theta_0 = \arctan(\alpha/\beta)$. Moreover, $\sqrt{\alpha^2+\beta^2} \le 1/2$ since the condition $h \le \lambda/10$ is usually met in practical FDTD simulations. Also, since $|J_n(x)| < 1/(2^n \cdot n!)$ for $|x| < 1$, the contributions of the higher order neglected terms decrease rapidly as the order increases, i.e., if additional H_z and/or h_z are used in the interpolation scheme. By using two values of H_z and one value of h_z, the first three most significant terms in the coupling error are made equal to zero, as enforced by (7).

After solving the integrals in (7), we obtain

$$\begin{bmatrix} J_0(\sqrt{5}kh/6) & J_0(\sqrt{17}kh/6) & J_0(kh/6) \\ J_1(\sqrt{5}kh/6)/\sqrt{5} & -2J_1(\sqrt{17}kh/6)/\sqrt{17} & 0 \\ J_1(\sqrt{5}kh/6)/\sqrt{5} & J_1(\sqrt{17}kh/6)/\sqrt{17} & -J_1(kh/6) \end{bmatrix} \cdot \begin{bmatrix} C_1 \\ C_2 \\ C_3 \end{bmatrix} = \begin{bmatrix} 0 \\ 0 \\ -i\eta/2 \end{bmatrix}. \quad (9)$$

Solving for C_1, C_2, and C_3 yields

$$\begin{aligned} C_1 =& -j\sqrt{85}\eta J_1\left(\sqrt{17}kh/6\right)J_0\left(kh/6\right)\Big/ \\ & \Big[17J_0\left(\sqrt{17}kh/6\right)J_1\left(kh/6\right)J_1\left(\sqrt{5}kh/6\right) \\ & + 2\sqrt{85}J_0\left(\sqrt{5}kh/6\right)J_1\left(kh/6\right)J_1\left(\sqrt{17}kh/6\right) \\ & + 3\sqrt{17}J_1\left(\sqrt{17}kh/6\right)J_0\left(kh/6\right)J_1\left(\sqrt{5}kh/6\right)\Big] \\ C_2 =& -j\sqrt{85}\eta J_0\left(kh/6\right)J_1\left(\sqrt{5}kh/6\right)\Big/ \\ & \Big[2\sqrt{85}J_0\left(\sqrt{17}kh/6\right)J_1\left(kh/6\right)J_1\left(\sqrt{5}kh/6\right) \\ & + 80J_0\left(\sqrt{5}kh/6\right)J_1\left(kh/6\right)J_1\left(\sqrt{17}kh/6\right) \\ & + 6\sqrt{5}J_1\left(\sqrt{17}kh/6\right)J_0\left(kh/6\right)J_1\left(\sqrt{5}kh/6\right)\Big] \\ C_3 =& j\eta\Big[\sqrt{17}J_0\left(\sqrt{17}kh/6\right)J_1\left(\sqrt{5}kh/6\right) \\ & + 2\sqrt{5}J_1\left(\sqrt{17}kh/6\right)J_0\left(\sqrt{5}kh/6\right)\Big]\Big/ \\ & \Big[2\sqrt{17}J_0\left(\sqrt{17}kh/6\right)J_1\left(kh/6\right)J_1\left(\sqrt{5}kh/6\right) \\ & + 4\sqrt{5}J_0\left(\sqrt{5}kh/6\right)J_1\left(kh/6\right)J_1\left(\sqrt{17}kh/6\right) \\ & + 6J_1\left(\sqrt{17}kh/6\right)J_0\left(kh/6\right)J_1\left(\sqrt{5}kh/6\right)\Big]. \end{aligned} \quad (10)$$

By expanding (10) in a Taylor series on kh and transforming the results to time domain, we obtain

$$\begin{aligned} j\omega h\epsilon C_1/3 &\to 2/3 - (1/24\chi^2)\Delta t^2\partial_t^2 + \mathrm{O}((kh)^4) \\ j\omega h\epsilon C_2/3 &\to 1/3 - (7/144\chi^2)\Delta t^2\partial_t^2 + \mathrm{O}((kh)^4) \\ j\omega h\epsilon C_3/3 &\to -1 - (1/48\chi^2)\Delta t^2\partial_t^2 + \mathrm{O}((kh)^4) \end{aligned} \quad (11)$$

where χ is the coarse region CFL number, Δt is the discrete time step, ω is the angular frequency, and ϵ is the permittivity. Note that in deriving the above equations, we have applied the following identities

$$\chi = \sqrt{2}\,\frac{c\Delta t}{h}$$
$$kh = \frac{\omega}{c}\,h = \omega\,\frac{\sqrt{2}}{\chi}\,\Delta t. \quad (12)$$

The coefficients in (11) are normalized so that the right hand sides can be inserted in the FDTD update directly. The second order time derivatives in (11) can also be replaced by second order space derivatives via Helmholtz equation. The derivative terms can be though of as dispersion correction terms which compensate for the difference in propagation constants and impedances between the fine and coarse regions. By dropping the second order time derivatives in C_1, C_2, and C_3, the scheme would reduce to a simple linear interpolation of an elliptic equation (static limit or conventional subgridding).

B. Higher Order, Five-Point Coupling Scheme

Higher order subgridding schemes utilize more than three points for the nearest neighbor coupling in (1). We have also examined five-point layout schemes. The optimized coefficients for a given five-point layout scheme can be derived in a similar way as done before for the three-point scheme. While different

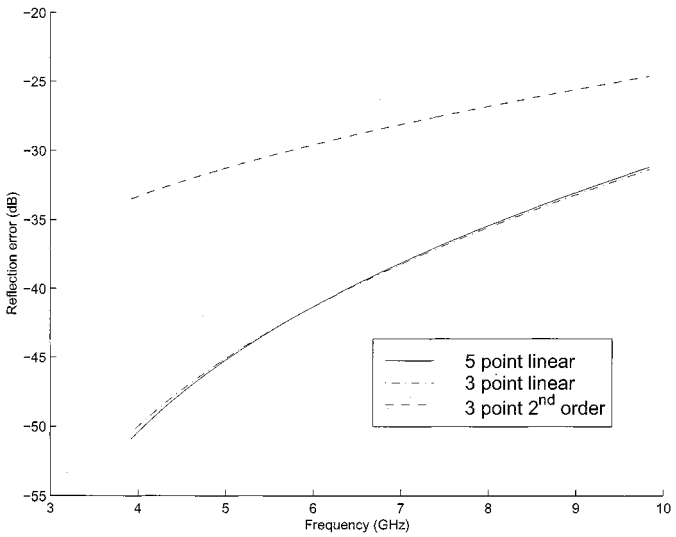

Fig. 2. Reflection levels at 0°.

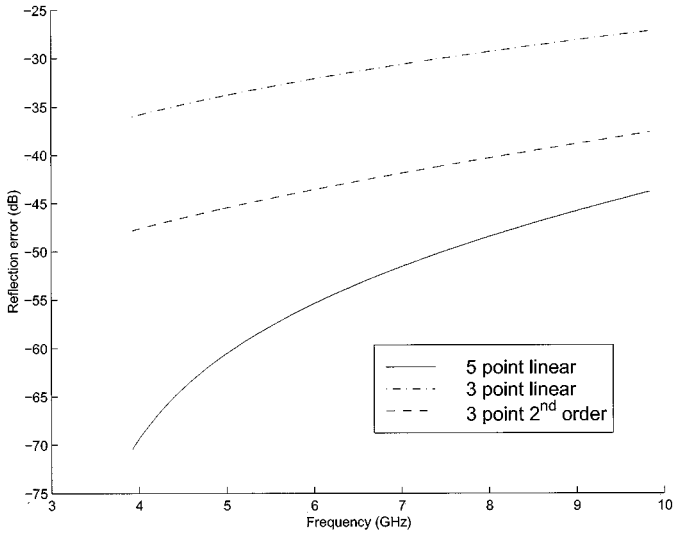

Fig. 3. Reflection levels at 45°.

five-point coupling layouts are possible, a satisfactory one uses two extra values for H_z in the coarse region, *viz.*, one at the grid point directly below H_{z1} and the other at the grid point directly above H_{z2} in Fig. 1. An equation similar to (6) (now with five coefficients to solve for) can then be obtained, whose coefficients are solved using an ansatz similar to (7), now also involving projections on $\sin(2\theta)$ and $\cos(2\theta)$ also. As mentioned before, the use of more points allows for these additional terms in the Fourier expansion of the coupling error to be made equal to zero, and hence produce a smaller overall residual error. The obvious drawbacks are loss of sparsity and increased computational cost.

IV. Numerical Results

We have run simulations on a coarse-fine region boundary of large FDTD domains avoiding interference from the corners and the mesh termination. Figs. 2 and 3 show the spurious relative reflection levels from the subgridding boundary as a function of frequency and angle. The cell size is equal to $\lambda/10$ at the highest frequency considered, $f = 10$ GHz, and the CFL number is $\chi = 1.0$ (fine region value).

From Fig. 2, we observe that, at small incidence angles, the three-point linear interpolation has a performance comparable to the five-point linear interpolation. This is expected because for plane wave normal incidence, a larger stencil on the transverse direction is not important. For oblique incidence angles, the performance of the three-point linear interpolation deteriorates. On the other hand, if the second order derivative terms are used, the performance is better than linear interpolation at 45°, but deteriorates at 0°, exhibiting complementary behavior according to the incident angle. This behavior can be explored when implementing subgridding schemes in different regions of a FDTD grid. As expected, the five-point linear interpolation has a smaller spurious reflection overall and largest reflection levels at 0°. Note that the ansatz in (7) is not unique or not necessarily optimal in any problem. Other possibilities could also be explored. In particular, any a priori information about the geometry of the problem, if available, can be used in designing different schemes.

V. Conclusion

Subgridding schemes are plagued by spurious reflections caused by the mismatch of the (discrete) wavenumbers and impedances between the coarse and fine meshes. In this work, we have introduced a procedure to reduce such reflections. Results from the application of the procedure to a $3:1$ subgridding algorithm in 2-D FDTD have shown that the spurious reflections can be minimized for different angles in a wide range of frequencies.

References

[1] A. Taflove, Ed., *Advances in Computational Electrodynamics: The Finite-Difference Time-Domain Method*. Boston, MA: Artech House, 1998.

[2] S. S. Zivanovic, K. S. Yee, and K. K. Mei, "A subgridding method for the time-domain finite-difference method to solve Maxwell's equations," *IEEE Trans. Microwave Theory Tech.*, vol. 39, pp. 471–479, Mar. 1991.

[3] M. Okoniewski, E. Okoniewski, and M. A. Stuchly, "Three-dimensional subgridding algorithm for FDTD," *IEEE Trans. Antennas Propagat.*, vol. 45, pp. 422–429, Mar. 1997.

[4] M. W. Chevalier, R. J. Luebbers, and V. P. Cable, "FDTD local grid with material transverse," *IEEE Trans. Antennas Propagat.*, vol. 45, pp. 411–421, Mar. 1997.

[5] W. Yu and R. Mittra, "A new subgridding method for the finite-difference time-domain (FDTD) algorithm," *Microwave Opt. Technol. Lett.*, vol. 21, no. 5, pp. 330–333, 1999.

[6] F. L. Teixeira and W. C. Chew, "Lattice electromagnetic theory form a topological viewpoint," *J. Math. Phys.*, vol. 40, no. 1, pp. 169–187, 1999.

[7] P. Thoma and T. Weiland, "A consistent subgridding scheme for the finite difference time domain method," *Int. J. Num. Model.: Electron. Network, Devices Fields*, vol. 9, pp. 359–374, 1996.